



## Article

# Thixoforming of the Hot Extruded Aluminum AlSi9Cu3(Fe) Machining Chips

Jure Krolo <sup>1,\*</sup> , Ivana Dumanić Labetić <sup>1</sup>, Branimir Lela <sup>1</sup>  and Martin Bilušić <sup>2</sup><sup>1</sup> Faculty of Electrical Engineering, Mechanical Engineering and Naval Architecture, University of Split, Ruđera Boškovića 32, 21000 Split, Croatia<sup>2</sup> AluTech, Velimira Škorpika 6, 22000 Šibenik, Croatia

\* Correspondence: jkrolo@fesb.hr

**Abstract:** The main aim of this research was to investigate the aluminum AlSi9Cu3(Fe) machining chips recycling possibility utilizing a direct hot extrusion process and thixoforming. The thixo feedstock was prepared directly from the aluminum alloy AlSi9Cu3(Fe) machining chips waste without any remelting step. The machining chips were compacted, and direct hot extruded to create the solid samples and thixo feedstock. The aluminum alloy AlSi9Cu3(Fe) machining chips had a high degree of plastic deformation and after extrusion and heating in the semisolid temperature range, the suitable globular microstructure was achieved, which is a precondition for a successful thixoforming process. This approach can be characterized as a semisolid recycling process with a lower energy consumption, a higher material yield, and reduced greenhouse gas emissions into the atmosphere compared with conventional casting and recycling. Optical metallography, scanning electron microscopy accompanied with energy dispersive spectroscopy, electrical conductivity, and mechanical properties investigation were performed on the reference casted sample with a dendritic microstructure, the extruded sample with a severely deformed microstructure, and finally the thixoformed samples with a globular microstructure produced with different parameters, according to the Taguchi L4 (2<sup>3</sup>) experimental plan.

**Keywords:** aluminum; thixoforming; machining chips; semisolid recycling; Taguchi method



**Citation:** Krolo, J.; Dumanić Labetić, I.; Lela, B.; Bilušić, M. Thixoforming of the Hot Extruded Aluminum AlSi9Cu3(Fe) Machining Chips. *Metals* **2024**, *14*, 796. <https://doi.org/10.3390/met14070796>

Academic Editor: Umberto Prisco

Received: 14 June 2024

Revised: 2 July 2024

Accepted: 5 July 2024

Published: 8 July 2024



**Copyright:** © 2024 by the authors. Licensee MDPI, Basel, Switzerland. This article is an open access article distributed under the terms and conditions of the Creative Commons Attribution (CC BY) license (<https://creativecommons.org/licenses/by/4.0/>).

## 1. Introduction

The processing of alloys and composites in a semisolid state plays a crucial role in contemporary manufacturing, particularly in the production of automobile, aviation, and marine components [1]. Semisolid metal processing (SSM) is a manufacturing technique that involves the processing of metal alloys in a state between a solid and a liquid, typically at temperatures within the mushy or semisolid range. This range lies between the solidus and the liquidus temperatures. The SSM processing methods combine the advantages of both solid-state forming (such as forging) and liquid-state forming (such as casting) [2]. To take advantage, it is necessary to obtain nondendritic (globular) structures, solid particles, and surrounding fluid acting as a lubricant in the mushy state of the metal. Thixotropic flow and plastic flow exist simultaneously due to the coexistence of a liquid and a solid in semisolid processing [3]. This specific microstructure results in a reduced resistance to flow, leading to a lower viscosity, which allows for better die filling and minimizes the risk of gas entrapment. This can result in the production of near-net-shaped components with a lower flow shrinkage porosity and reduced thermal stress [4–6]. In addition, due to the reduced forming load, SSM processing can be more energy efficient compared with traditional forging methods [2,7]. In addition, the use of partially solidified material during filling can contribute to an increased die life by minimizing the thermal shock, and the cycle time in SSM processing can be significantly reduced compared with traditional casting methods, contributing to overall production efficiency [8]. There are numerous techniques

for achieving the thixotropic properties of slurries, i.e., for the production of the described microstructure of the slurry. These methods can be classified into two primary categories: rheo processes and thixo processes. Rheo processes include creating the semisolid slurry directly from a liquid phase, while thixo processes involve the preparation of feedstock material (usually by introducing a high degree of plastic deformation), reheating and forming. It is crucial to emphasize that the morphology, such as the circularity, and the size of these globules have an impact on the properties and the performance of the components [9]; therefore, it is important to control both the size and the shape of the globules. The rheological behavior during processing improves with smaller globule sizes (GS) and a larger circularity of the globules, as indicated by various studies [10,11].

Some authors have investigated the A380 aluminum alloy [4,12–20]. Das et al. [12] obtained spherical solid grains (primary  $\alpha$ -Al crystals) using the Cooling Slope (CS) process. Fabrizi et al. [4] and Gecu et al. [13] investigated the effect of heat treatment (T6) on the microstructure and hardness using the Swirled Enthalpy Equilibration Device (SEED) and Low Superheat Casting (LSC) processes, respectively. The average GS was 70  $\mu\text{m}$  [4]. Parshizfard and Shabestari [14] achieved a GS from 70  $\mu\text{m}$  to 90  $\mu\text{m}$  and a shape factor (SF) of 0.79 using the strain-induced melt-activating (SIMA) process. They varied the plastic deformation and holding times in the semisolid temperature range. In the study conducted by Gencalp and Saklakoglu [15], the most suitable microstructure of A380 was achieved by reheating at 567  $^{\circ}\text{C}$  for 5 min, resulting in an SF of 0.892. This was achieved through the application of CS casting under a vibration process. Guo et al. [16] employed the Rheo-Diecasting (RDC) process and obtained a GS between 30  $\mu\text{m}$  and 50  $\mu\text{m}$  and an SF between 0.89 and 0.91. Typically, a globule size below 100  $\mu\text{m}$  is considered preferable [10].

By utilizing the Equal Channel Angular Pressing (ECAP) thixo feedstock preparation, Proni et al. [11] obtained Al5Si2.8Cu, Al6Si2.8Cu, and Al7Si2.8Cu samples with a GS of 55  $\mu\text{m}$  and an SF of more than 0.60. With the same technique, Fu et al. [21] observed a 55  $\mu\text{m}$  globule size and 0.82 circularity for the 7075 aluminum alloy. Meshakabadi [22] reported slightly larger globules (70–100  $\mu\text{m}$ ) with a circularity of 0.62 for the A356 alloy. Yang et al. [23] produced a 6061 aluminum alloy thixo feedstock using the ECAP–RAP process. They utilized the response surface methodology to find the optimal holding temperature and holding time for the desirable microstructural characteristics, which were 623  $^{\circ}\text{C}$  and 13 min, respectively. This resulted in a GS of 35.97  $\mu\text{m}$  and an average SF of 0.8535. Ch et al. [24] concluded that an extrusion ratio (ratio of the extrusion cylinder and the orifice diameter) was the most significant parameter for achieving a higher tensile strength and percentage of elongation in the thixo-extrusion of the AA2017 alloy. Dantas et al. [25] determined that the Al-Si-Zn-Mg alloy was suitable for thixoforming due to the appropriate rheological behavior during the open-die forging (maximum engineering stress and apparent viscosity). Wang et al. [26] concluded that a higher amount and more uniform distribution of the inter-granular microstructure in the tensile samples resulted in increased tensile strength and an elongation of the 7075 aluminum alloy samples. The tensile samples were taken from the cup-shaped parts produced by compression molding of the extruded parts in the semisolid range.

In this research, the selected material for recycling was the aluminum alloy AlSi9Cu3(Fe). The aluminum–silicon casting alloys play a crucial role in the automotive industry, owing to their good corrosion resistance, mechanical properties, ability to resist hot cracking, and lightweight nature [4]. Often, aluminum alloys are manufactured through traditional casting and finished with the manufacturing process, resulting in a substantial volume of waste in the form of aluminum chips [27]. It is well known that aluminum alloy recycling is crucial for environmental pollution reduction and the conservation of electrical energy. Lately, new recycling techniques based on direct material recycling without remelting are gaining more attention [28–32]. The benefits of semisolid aluminum machining chips recycling are numerous. The primary aluminum production process is a high-energy consumption process that uses approximately 160 GJ per ton. On the other hand, secondary aluminum production processes use only about 10 GJ per ton, which depends on the waste

type [33]. During the conventional recycling of machining chips using remelting, a great deal of material can be lost due to the high surface-to-mass ratio, oxidation, slag formation, etc. [34].

To eliminate the remelting and poor material yield during conventional recycling, semisolid metal processing (thixoforming) has been used in this research as the recycling process, i.e., the semisolid recycling process. Due to the specific microstructure characteristics of the aluminum machining chips, this type of waste should be an excellent starting material to produce the thixo feedstock material. In the machining chips, the casts' dendritic microstructure undergoes a significant deformation and distortion, accompanied by the shredding and refinement of the intermetallic compounds during machining, resulting in cold work affecting the entire volume [19,35]. Upon heating, the chips undergo substantial microstructural changes, transitioning from a cold-deformed structure to one characterized by strain-free grains [36]. Reheating the metal waste above the solidus temperature has a high potential to transform the highly deformed structure into a globular form that is suitable for the thixoforming process, making it a quite promising starting material for such applications. Based on the authors' available literature, it appears that there are a limited number of studies on the semisolid metal waste recycling technique.

Wang et al. [37,38] conducted a series of studies exploring the potential for recycling the aluminum alloy A383 chips in the semisolid state. The process involved placing the chip in a cylinder mold and heating it to a temperature of 200 °C. Subsequently, the metal was pressed in the mold, resulting in billets. These billets were then heated within a range between the solidus and liquidus temperatures of the alloy and subsequently cooled in water. This process led to the observation of a globular microstructure in the samples, confirming the feasibility of recycling alloy A383 using this method [37]. In a subsequent study, Wang et al. [38] optimized the treatment process, determining that the optimal heating temperature for the A383 billets was 555 °C, with a 30-min holding time, achieving the optimum globular phase size and circularity. Wang et al. [39] explored the influence of temperature and heating time on a slurry made of chips from the aluminum alloy A356. After compressing the chips at a compression temperature of 400 °C, the chips were heated to a temperature within the semisolid range and then rapidly cooled in water. The study identified that the best combination of grain size and circularity of the  $\alpha$ -Al grains was achieved at a heating temperature of 600 °C and a heating time of 15 min. Wang et al. [40] concluded that the optimal isothermal treatment temperature was 620 °C and the holding time was 3000 s for the roundness and grain size. The Al-Cu-Mn-Ti aluminum alloy chip was used to prepare the semisolid billet using the SIMA method. In both studies, it was concluded that it was indeed possible to create a high-quality thixo feedstock by utilizing metal waste, demonstrating the potential for sustainable recycling and resource efficiency in aluminum alloy processing. Son et al. [41] delved into the microstructure and mechanical properties of the samples created from the uniaxially pressed aluminum alloy chips (Al-8Zn-6Si-4Mg-2Cu). Utilizing a pressure-less process (the pressure released from 80 MPa to 0 MPa at 450 °C) enabled the fabrication of the samples with a globular microstructure after heating in the semisolid range. Process parameters, such as temperature, pressure, and holding time, at semisolid temperature were investigated to achieve the suitable relative densities and compressive strength. The densities of the final samples increased with the holding time at a semisolid temperature, but the compressive strength was reduced. Gudić et al. [19] showed that the semisolid recycling of the AlSi9Cu3(Fe) machining chips could produce a globular microstructure thixoformed material with an increased corrosion resistance compared with the conventionally recycled specimens.

The semisolid metal waste recycling technique could be a promising recycling approach, reducing the limitations of the conventional recycling and increasing both the environmental and economic benefits. The method could be described as an innovative process, with a lower energy consumption and less greenhouse gas emissions into the atmosphere, but with an increased material yield compared with conventional recycling due to avoiding the remelting of the metal. In addition, from the literature overview, it

was evident that there is space for additional research focusing on the determination of suitable process parameters for the globular microstructure formation and the possibility of performing thixoforming of the chips-based thixo feedstock.

To perform the semisolid recycling and thixoforming in this research, the aluminum alloy AlSi9Cu3(Fe) machining chips were compacted, and direct hot extruded to create the solid samples and the thixo feedstock material with a highly deformed microstructure and extremely refined intermetallic compounds and crystal grains. The thixo feedstock aluminum bars were heated at an appropriate semisolid temperature range and the thixoforming process was performed to obtain the semi-finished recycled specimens. The quality of the obtained semisolid recycled specimens was determined utilizing optical microscopy and scanning electron microscopy accompanied by energy dispersive X-ray spectroscopy, which served to determine the globule formation and intermetallic compound distribution and size. The mentioned analysis was also performed on the conventionally casted specimen and extruded thixo feedstock specimen to compare the microstructural characteristics. Furthermore, to investigate the mechanical and electrical properties of the semisolid recycled (thixoformed) specimens and to compare them with the casted and chip-based extruded (thixo feedstock) specimens, the tensile test, hardness, and electrical conductivity analysis were performed. Finally, to further and in more detail investigate the influence of the different thixoforming parameters, Taguchi's L4 ( $2^3$ ) experimental plan was performed. The Taguchi method is frequently utilized to determine the optimal processing parameters and to provide a more detailed description of the manufacturing processes research [42–44]. For the thixoforming parameters chip sizes, the semisolid temperatures and holding times within the semisolid range were variated at two levels. The grey relational analysis was utilized to identify the optimal process parameters for thixoforming for a multi-objective function.

## 2. Materials and Methods

The main aim of this research was to determine the recycling possibility of the EN AC aluminum alloy machining chips to produce cost-effective thixoformed samples. To investigate the possibility of the thixoforming of the aluminum chips, the first step was to select a suitable alloy and to prepare the machining chips. The selected alloy was EN AC AlSi9Cu3(Fe) similar to EN AC 44000, DIN 226, or A 380 depending on the used standard, and it was obtained from Aluminij Industries d.o.o., Mostar, Bosnia and Hercegovina. The chemical composition of the alloy was determined using a GDS500A LECO optical emission spectrometer (LECO Corporation, St. Joseph, MO, USA), Table 1.

**Table 1.** Chemical composition of the aluminum alloy EN AC AlSi9Cu3(Fe) batch.

Cu %	Si %	Fe %	Mn %	Mg %	Zn %	Cr %	Ni %	Pb %	Others %	Al %
3.486	10.45	1.24	0.258	0.303	0.966	0.0453	0.043	0.141	0.11	Bal.

This alloy has a wide range of applications and there is a lot of machining chips waste generated from this alloy. According to various authors [10,45,46], this alloy can be used in semisolid metal processing. The alloy was obtained in the form of the casting ingots, and they were machined using the Spinner VC 560 vertical machining (SPINNER GmbH, München, Germany) center using a depth of cut, cutting speed, and feed rate of  $a_p = 1.5$  mm,  $v_c = 120$  m/min, and  $f = 0.1$  mm/tooth, respectively. To avoid contamination with the cooling and lubrication fluid, a dry face milling process was performed using a tool composed of the WALTER (Walter AG, Tübingen, Germany) tool holder with designation M4132-032-W32-02-09 and the SDHT09T304-G88 WK10 cutting insert. The obtained aluminum milled chips were weighted to a mass of 150 g and compacted in a cylindrical steel tool with an inner channel diameter of 38 mm. A compaction force of 300 kN was used, and the compacted billets with 38 mm in diameter and 68 mm in height were obtained. The compaction was performed on a 1 MN universal hydraulic press, with the force measured using the HBM load cell C6A 1 MN sensor (HBM, Darmstadt,



Germany). After the compaction step, in order to produce a consistent and solid thixo feedstock, the direct hot extrusion process was utilized. The chip-based billets were preheated for 20 min at 450 °C, placed in an extrusion cylinder with a diameter of 40 mm, and directly hot extruded at 400 °C with a 7.1 extrusion ratio. A flat die with an orifice diameter of 15 mm was used in the extrusion process. The billet preheating time should be long enough for the billet to heat up through the whole volume, otherwise, increased extrusion forces could occur due to the increased flow stress of the aluminum alloy. The flow stress will also increase if a too low extrusion temperature is selected and usually those temperatures are above 400 °C [47]. Furthermore, according to previous research, higher extrusion temperatures are desirable to obtain better chip bonding due to the reduced flow stress of the material and better diffusion bonding [48]. On the other hand, for this specific alloy AlSi9Cu3(Fe) there is a possibility of blisters development during the heat treatment at a temperature higher than 500 °C [49]. Therefore, to prevent possible blisters formation, but to ensure good chips bonding, a 400 °C temperature was selected, while the preheating time was 450 °C due to some heat dissipation during transport to the extrusion cylinder. A schematic representation of the utilized direct hot extrusion process is presented in Figure 1a. The punch speed was 1 mm/s. The temperature was controlled using the Omron E5CC (Omron Corporation, Kyoto, Japan) temperature regulator and G3PE-225B DC12-24 relay (Omron Corporation, Kyoto, Japan). The extrusion pressure was measured using an HBM P15RVA1/500B (HBM, Darmstadt, Germany) pressure gauge transducer. The extruded profiles were about 300 mm long, and they were cut on smaller 100 mm length thixo feedstock bars. Finally, the SSM tool and the extruded thixo feedstock bars were heated at an appropriate thixoforming temperature and thixoformed in the SSM tool presented in Figure 1b.

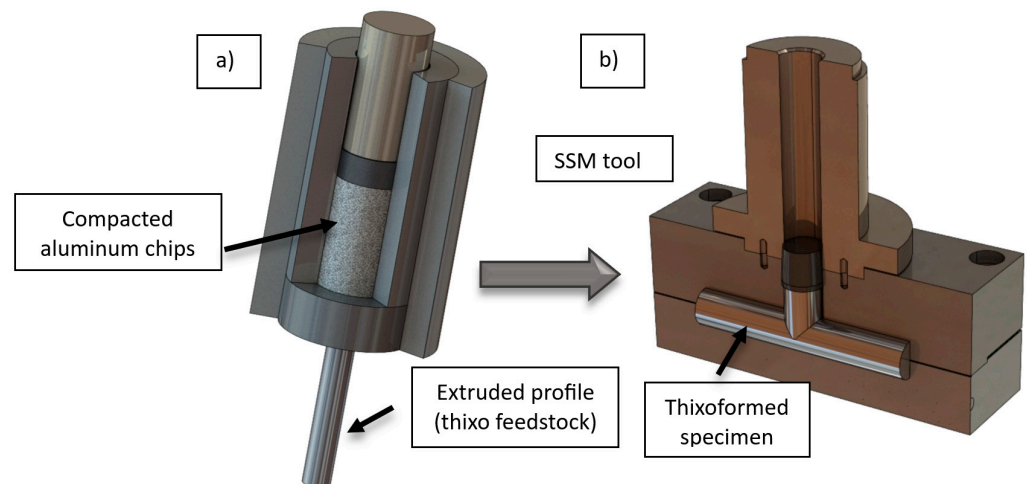


**Figure 1.** Schematic representation of the semisolid recycling process: (a) direct hot extrusion; (b) thixoforming.

The thixoforming temperatures were selected according to the Thermo-calc 2022a computer software and classical Shiel diagram for the aluminum alloy EN AC AlSi9Cu3(Fe) and the chemical composition from Table 1, Figure 2. According to the previous research and differential scanning calorimetry (DSC) analysis of the EN AC AlSi9Cu3(Fe) aluminum alloy, it was suitable to choose a temperature of approximately 567 °C to achieve a 40% to 50% solid phase in the semisolid slurry [45,50,51]. According to Birol et al., the penetration of the thermocouple into the slug, taken as a sign of thixoformability, occurred at 568 °C. Furthermore, once the temperature exceeded 572 °C, the slugs were no longer able to sustain their own weight and were deformed too much [51]. According to the diagram presented in Figure 2, 50% to 30% of the mass of solid phase in the semisolid slurry should be achieved at temperatures between approximately 560 °C and 566 °C. However, the experiments in this research showed that appropriate globule formation was achieved at a

temperature from 568 °C to 575 °C of the SSM tool, which are higher temperatures than suggested with the Shiel diagram. The surface temperature of the SSM tool was measured using a contact thermometer DT02 and type K thermocouple probe because it was not possible to measure the slurry directly. Furthermore, due to the fact that the thixo feedstock material was made of the machining chips of the mentioned alloy, which had an increased aluminum oxide concentration, this could also be a reason for the increased temperature of the globule formation. According to the results of this research, a holding time of at least 10 min in the mentioned range should be applied in order to achieve the globular microstructure, while too-long holding time led to globule coagulation and overgrowth and porosity development. The optimal parameters are yet to be determined.

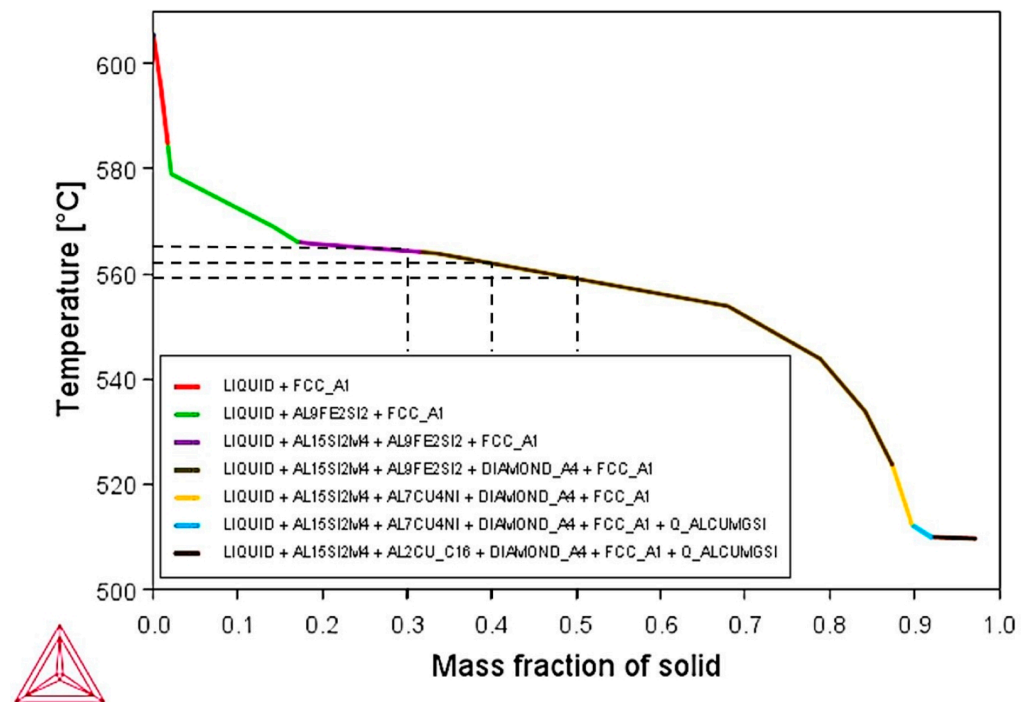


**Figure 2.** Thermo Calc classical Shiel diagram for the aluminum alloy EN AC AlSi9Cu3(Fe).

For the optical microscopy, the samples were etched electrolytically with Barker's reagent (2.5% HBF<sub>4</sub> in water) at 23 V for 1 min. The microstructure was characterized using polarized light using an Olympus BX61 optical microscope (Olympus, Tokyo, Japan). For the additional optical metallography analysis, an optical microscope "OPTON Axioskop" (Germany) and computer software "DinoCapture 2.0" were utilized. The samples were etched with a reagent that consisted of 0.5 mL of 40% HF (Hydrofluoric Acid) dissolved in 100 mL of water for a duration of 40 s at room temperature. The ImageJ free analysis software (ImageJ/Fiji 1.46) was utilized to determine a globule diameter ( $D_{eq}$ ) and circularity shape factor ( $SF$ ) of the primary  $\alpha$ -Al globules by applying Equations (1) and (2), respectively [52]:

$$D = \sum_{i=1}^N \frac{\sqrt{4A_i/\pi}}{N} \quad (1)$$

$$SF = \sum_{i=1}^N \frac{4\pi A_i}{P_i^2} \quad (2)$$

where  $A_i$  is the surface area of the globule  $i$ ,  $N$  is the number of globules, and  $P_i$  is the perimeter of the globule  $i$ . The globule size is given by the globule diameter  $D_{eq}$ . If the solid globules were perfectly circular, the  $SF$  value was one. At least 50 globules were taken into account for each specimen. The scanning electron microscopy (SEM) and energy dispersion spectroscopy (EDS) analyses were performed using the Thermo Scientific Quattro S Field

Emission Scanning Electron Microscope (FEG SEM, Hillsboro, OR, USA) in conjunction with the Ultim Max 65 SSD energy dispersive X-ray spectrometer from Oxford Instruments and the Aztec software platform ver. 6.0 (Abingdon, UK). The electrical conductivity of the alloy was measured at room temperature using the eddy current method on the Olympus NORTEC 600C (Olympus, Tokyo, Japan) device. The electrical conductivity was expressed as IACS (%), which stands for the International Annealed Copper Standard. At least five electrical conductivity measurements were taken for each sample and the arithmetic value was taken as the final. The microhardness testing was performed according to the HR EN ISO 6507-1:2018 standard [53] for metal material microhardness testing. The used device was a Shimadzu HMV-2T (Shimadzu, Kyoto, Japan) universal machine with an integrated DynoLITE camera for the computer software analysis. The microhardness was measured utilizing the Micro Vickers method with an applied force of 9.8 N for a duration of 10 s at room temperature. At least five microhardness measurements were taken for each sample and the arithmetic value was taken as the final. A tensile test was performed on the Raagen universal tensile test machine ETM-250-S with a maximum force of 250 kN (Ankara, Turkey). The specimens were prepared following the HRN EN 10002-1 [54] norm with a reduced section diameter of 5 mm.

### 3. Results and Discussion

#### 3.1. Optical Microscopy

An optical microscopy analysis was performed on the casted commercial specimen (reference specimen), the extruded machining chips waste (thixo feedstock), and the semisolid recycled (thixoformed) specimen, Figure 3. The thixoformed sample in this case was obtained using a temperature of 570 °C and 15 min of heating time. Figure 3a shows the classic dendritic microstructure of the casted specimen; however, Figure 3b shows the unique microstructure of the extruded machining chips, with refined crystal grains and intermetallic compounds. Finally, Figure 3c shows the microstructure of the thixoformed specimen. It is visible that a globular microstructure was achieved. Therefore, it was confirmed that compacted and direct hot extruded machining chips can be appropriate thixo feedstock material when the goal is to achieve thixotropic behavior (globular microstructure) of the material during thixoforming.

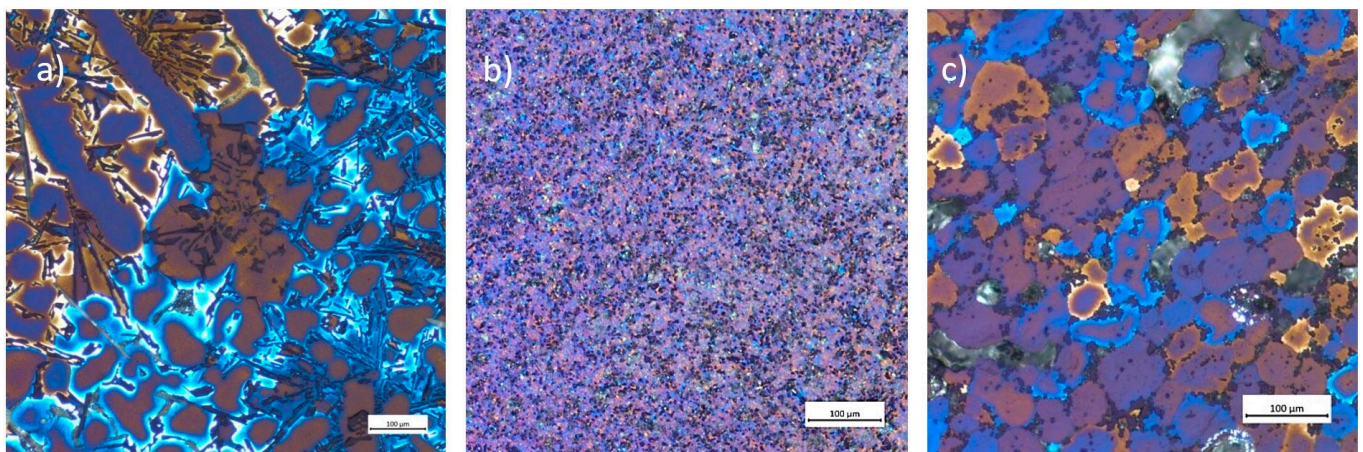


**Figure 3.** Optical microscopy analysis of the (a) casted specimen, (b) hot extruded specimen, (c) thixoformed specimen (specimens were etched electrolytically with Barker's reagent (2.5% HBF<sub>4</sub> in water) at 23 V for 1 min).

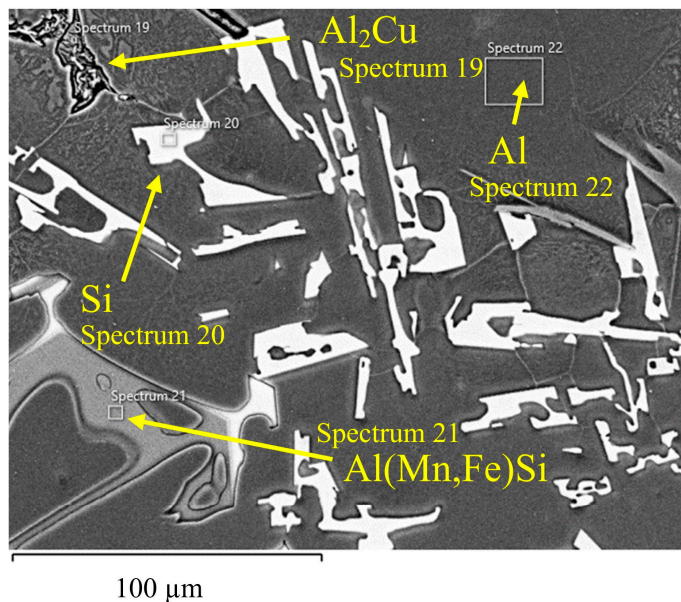
According to Figure 3c, the average globule size and circularity shape factor are 56 µm and 0.73, respectively.



### 3.2. Scanning Electron Microscopy and Energy Dispersive Spectroscopy

In continuation, the scanning electron microscopy analysis was accompanied by an energy-dispersive spectroscopy to identify the intermetallic compounds in the specimens and to determine their average size. According to the previous research, the dendritic  $\alpha$ -Al, morphology, and size of the eutectic silicon, and the morphology and composition of the intermetallic compounds should have a great impact on both the mechanical and physical properties of the specimens. Usually, formed phases are the primary aluminum, eutectic, and polyhedral silicon phases and additionally the Fe-rich and Cu-rich intermetallic phases [13,50]. According to the determined chemical composition of the used batch and the calculated Shiel diagram and stoichiometric calculations, the corresponding phases that should occur during the solidification were the dendritic network of primary  $\alpha$ -Al,  $\beta$ -AlFeSi,  $\beta$ Si,  $\text{Al}_{18}\text{Fe}_2\text{Mg}_7\text{Si}_{10}$ ,  $\theta$ - $\text{Al}_2\text{Cu}$ , and Q-AlCuMgSi.

Figure 4 shows the intermetallic compounds for the used aluminum alloy EN AC AlSi9Cu3(Fe) in the referent casted state. There was a formation of needle-like Fe-rich and silicon phase particles around the dendritic branches. Spectrum 19 confirmed the presence of the Cu-rich particles. Spectrum 20 confirmed the formation of the needle-like silicon phase particles. Also, the needle-like formation of the Fe-rich particles was noticed and confirmed with spectrum 21.



Spectrum Label	Spectrum 19	Spectrum 20	Spectrum 21	Spectrum 22
Al	67.98		51.32	89.35
Si	14.45	100.00	27.44	10.65
Cr			1.66	
Mn			4.81	
Fe			14.77	
Ni	1.31			
Cu	16.26			
Zn				
Total	100.00	100.00	100.00	100.00

**Figure 4.** SEM + EDS analysis of the casted specimen.

The iron-containing compounds that form during the solidification processes appear in a few shapes and sizes, usually divided into three different morphologies:  $\beta$ - $\text{Fe}_5\text{AlSi}$  needles,  $\alpha$ - $\text{Al}_{15}(\text{Mn,Fe})_3\text{Si}_2$ , and polyhedral crystals. Usually, iron is the major impurity element that influences the detrimental  $\beta$ -phase formation in secondary aluminum alloys [55]. The  $\beta$ - $\text{Fe}_5\text{AlSi}$  intermetallic compound is hard and brittle, having a low cohesion with the aluminum matrix. It acts as a crack initiator and plays a role in forming solidification defects, such as porosity and hot tearing. This can lead to the decreased mechanical properties of the cast components [50,55,56].

Figure 5 shows that in the thixo feedstock material, the intermetallic compounds were greatly refined compared with the casted specimen. The reason is that the thixo feedstock material was produced directly from the machining chips without any remelting step. During the machining process of the casted ingot, intensive plastic deformation was introduced into the machining chips, and during the chips formation, the intermetallic compounds were cut into smaller pieces. An additional deformation was introduced during the chips compaction step. Finally, the complex thermo-mechanical process of



the direct hot extrusion of the compacted chips resulted in the production of the chip-based thixo feedstock material with the microstructure presented in Figure 5. Spectrums 13 to 17 confirmed the formation of the same intermetallic compounds as in the casted specimen; however, all the intermetallic compounds had some polyhedral shape instead of a needle-like appearance. Furthermore, a homogeneous distribution of the highly refined intermetallic compounds could be observed.

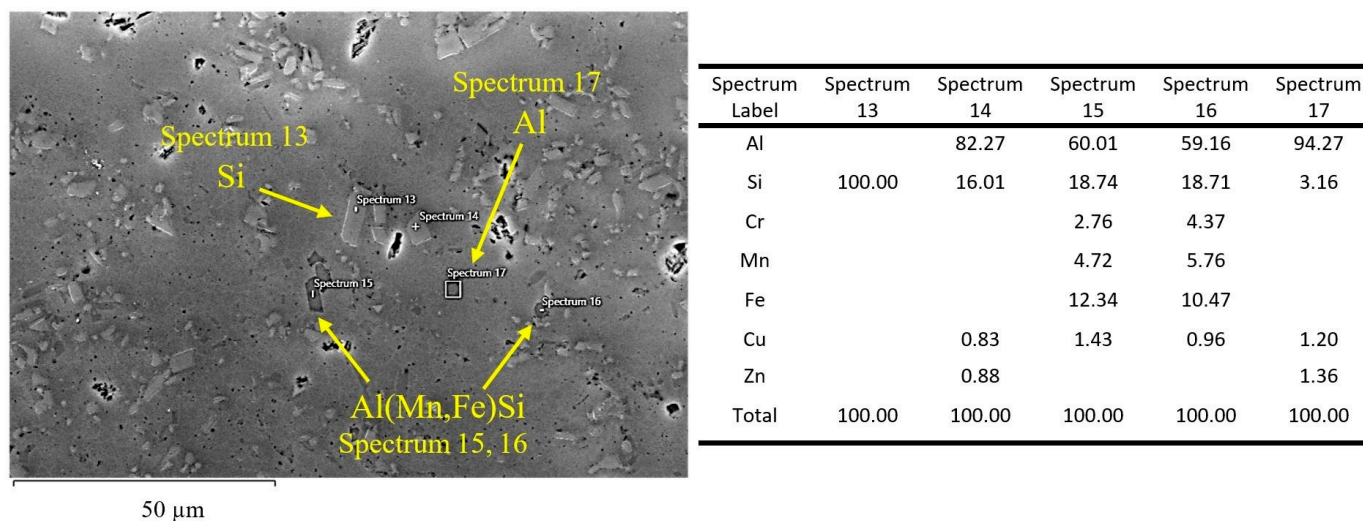


**Figure 5.** SEM + EDS analysis of the extruded chip-based thixo feedstock specimen.

Figure 6 shows that the polyhedral and refined appearance of the intermetallic compounds after the thixoforming process was preserved. Spectrums 1 and 2 indicate that silicon phase particles had a polyhedral shape, and that they were homogeneously distributed around the globular primary aluminum (spectrum 5). Similarly, spectrum 3 and 4 clearly indicated that the Fe-rich phases also had a polyhedral shape appearance and a similar homogeneous distribution around the globular primary aluminum.

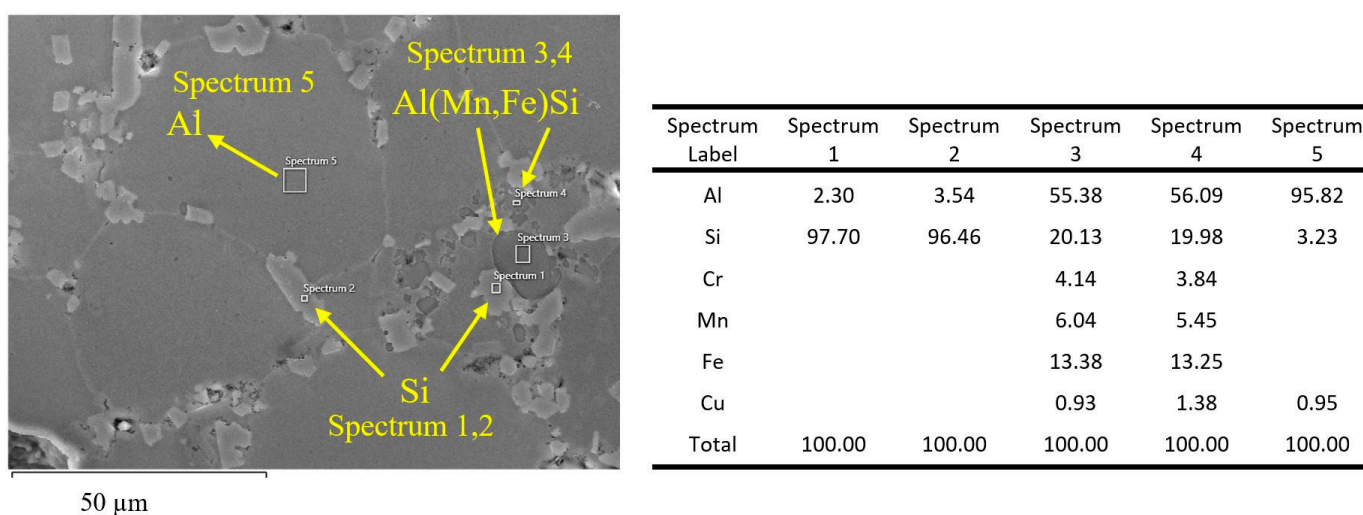


**Figure 6.** SEM + EDS analysis of the thixoformed specimen (570 °C, 15 min).

Figure 7 shows a scanning electron microscope accompanied by a qualitative analysis of the chemical elements mapping and distribution for the thixoformed specimen to examine in more detail the obtained intermetallic compounds. According to Figure 7, there is no evidence of any needle-like intermetallic compounds. Using a higher magnification in this case, some Cu-rich intermetallic compound presence was also confirmed. It seems that the oxygen distribution was homogeneous, which indicated that the increased aluminum oxide

content inside the recycled specimens was homogeneously dispersed during the complex semisolid recycling procedure presented in this research. According to previous research, if the machining chips aluminum oxide layer is not sufficiently broken into smaller pieces and homogeneously distributed inside the recycled specimens, deterioration of the mechanical properties can be observed [57].

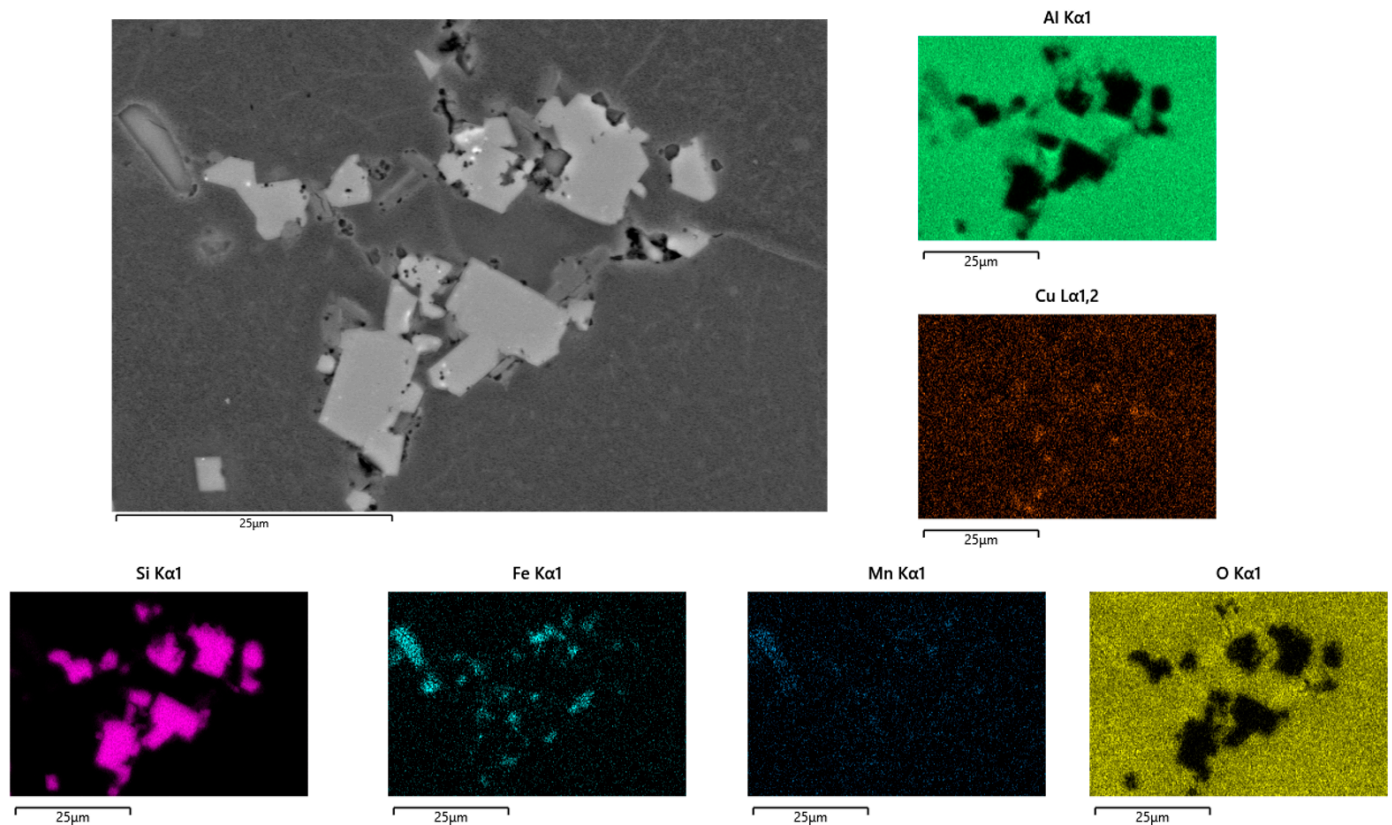


**Figure 7.** Thixoformed sample (570 °C, 15 min).

### 3.3. Mechanical and Physical Properties

To confirm the possible negative influence of the needle-like intermetallic compounds inside the cast (reference) specimen or the negative influence of the aluminum oxide and some possible microporosity inside the cast, extruded and thixoformed recycled specimen on the mechanical properties, microhardness and tensile testing were performed. Furthermore, to investigate the influence of the abovementioned electrical conductivity, measurement was also performed. In Table 2, the measurement results for the microhardness and electrical conductivity are presented.

**Table 2.** Microhardness and electrical conductivity measurement results.

Electrical Conductivity (%IACS)		
Casted 23.59	Extruded 31.46	Thixoformed 27.74
Hardness (HV)		
Casted 94.68	Extruded 67.08	Thixoformed 87.78

According to the results, the electrical conductivity and microhardness were significantly different depending on the used processing technology. The microhardness values were highest for the casted specimen, followed by the thixoformed recycled specimen,

and finally the extruded thixo feedstock material. In reverse order were the electrical conductivity measurement results. The electrical resistivity ( $\rho$ ) was inversely related to the electrical conductivity. Usually, the well-known Matthiessen's rule [58] is used to describe the electrical resistivity ( $\rho$ ) dependence of several microstructural features:

$$\rho = \rho_0 + \Delta\rho_S + \Delta\rho_P + \Delta\rho_V + \Delta\rho_D + \Delta\rho_B \quad (3)$$

where  $\rho_0$  describes the resistivity of the pure solvent metal and  $\Delta\rho$  stands for the increase in the electrical resistivity due to the atoms in the solid solution ( $S$ ), precipitates ( $P$ ), vacancies ( $V$ ), dislocation ( $D$ ), and grain boundaries ( $B$ ). According to the results, it seemed that in the thixo feedstock specimen (extruded), due to the processing at 400 °C, the solute atoms that were dissolved in the matrix (which are usually responsible for the enhanced precipitation hardening and reduced electrical conductivity) had enough time to diffuse out of the Al matrix and form overgrown precipitates. This is a reason for the reduced hardness and increased electrical conductivity compared with the casted and thixoformed specimens. It seems that the refined crystal grains and intermetallic compounds in the extruded samples, compared with the casted or thixoformed specimens, had a limited effect on the hardness and electrical conductivity. Higher processing temperatures during the casting process and thixoforming process (enough temperature for the solid solution), followed by relatively fast cooling on air, caused an increased hardness but a reduced electrical conductivity. The increased electrical conductivity but the reduced hardness of the thixoformed specimens compared with the casted specimen suggested that heat treatment could enhance the hardness of the recycled specimens, but that this will lead to reduced electrical conductivity. It is important to mention that due to the significant formation of the intermetallic compounds in the casted and thixoformed specimens, the microhardness values were measured on  $\alpha$ -Al dendritic crystal grains; therefore, a tensile test was performed for further comparison of the specimens. Table 3 presents the tensile testing results of the above-mentioned specimens.

**Table 3.** Tensile testing results.

Tensile Strength (MPa)		
Casted 161	Extruded 313	Thixoformed 293

According to the tensile test results, deformation during extrusion and the thixoforming process significantly increased the mechanical properties of the aluminum alloy EN AC AlSi9Cu3(Fe). This was due to the reduced porosity of the semisolid feedstock and the thixoformed specimen compared with the EN AC AlSi9Cu3(Fe) casted ingot. It is fair to say that if the referent aluminum alloy AlSi9Cu3(Fe) was processed with high-pressure die casting then the porosity would most likely be reduced and the mechanical properties increased; however, the overall tensile testing result from this research clearly indicated that the semisolid metal recycling method provided samples with promising mechanical properties.

### 3.4. Taguchi Method and Multi-Objective Optimization

To further and in more detail investigate the influence of the different thixoforming parameters, Taguchi's L4 ( $2^3$ ) experimental plan was performed. The chip sizes, semisolid temperature, and holding times within the semisolid range were selected as the controllable parameters for thixoforming. Each of these factors had two levels, as outlined in Table 4. The selection of the levels for the temperature and holding times is detailed in the experimental procedure section, leading to the choice of Taguchi's L4 ( $2^3$ ) orthogonal array for organizing the experimental design. The selected temperature range to obtain a suitable microstructure was from 568 °C to 575 °C. In addition, the holding times were selected to be from 10 min to 15 min. A third parameter in this research was the machining chip size, which could influence the degree of plastic deformation and intermetallic compounds refinement and

therefore potentially affect the mechanical and physical properties of the semisolid recycled specimens. The smaller chip size matched that of the thixoformed specimens in the previous section, with average dimensions of 2 mm width, 8.8 mm length, and 0.1 mm thickness, while the bigger size chips had an average width, length, and thickness of 3.9 mm, 8 mm, and 0.3 mm, respectively. The experimental plan is presented in Table 4. The microstructure characteristics, specifically the globule size and circularity, were used as outcome measures. Additionally, the mechanical and electrical properties of the thixoformed samples, such as tensile strength, electrical conductivity, and hardness were examined. The grey relational analysis (GRA) was employed to identify the optimal solution values of the multiple desired goals. The desirable characteristics for the thixoformed samples included a small globule size, and high circularity, tensile strength, electrical conductivity, and hardness values.

**Table 4.** Taguchi L4 ( $2^3$ ) experimental plan and selected thixoforming input parameters.

Run Order	Chip Size	Temperature (°C)	Time (min)
1	small	575	15
2	big	568	15
3	small	568	10
4	big	575	10

The experimental runs with the obtained testing results are presented in Table 5. The tensile strength, hardness, and electrical conductivity for the thixoformed specimens were in the range from 174 MPa to 267 MPa, 78.98 HV to 93.3 HV, and 26.37%IACS to 29.42%IACS, respectively. Globule size and circularity were in the range from 35.52  $\mu\text{m}$  to 71.20  $\mu\text{m}$  and 0.74 to 0.82, respectively. An average of five microhardness measurements were taken for each sample and the arithmetic value was taken as the final. The lobule size for all specimens fell into the results range of the previous research mentioned in the introduction section [4,10,14–16,21]. The obtained results were in accordance with the results obtained in Tables 2 and 3, and it is fair to claim that all the obtained specimens were successfully recycled. Based on these results for the four different semisolid recycled specimens, now it is possible to perform a multi-objective optimization and select the optimal semisolid recycling parameters in terms of this research scope.

**Table 5.** Output Taguchi L4 ( $2^3$ ) experimental plan parameters results.

Run Order	Tensile Strength MPa	Electrical Conductivity %IACS	Average Hardness HV	Globule Size $\mu\text{m}$	Circularity SF
1	267	28.29	78.98	37.60	0.75
2	174	26.37	93.3	93.59	0.82
3	250	29.42	88.68	35.52	0.74
4	245	29.42	91.52	71.20	0.77

Figure 8 presents the optical microscopy metallographs of the four specimens prepared according to the Taguchi L4 ( $2^3$ ) experimental plan.



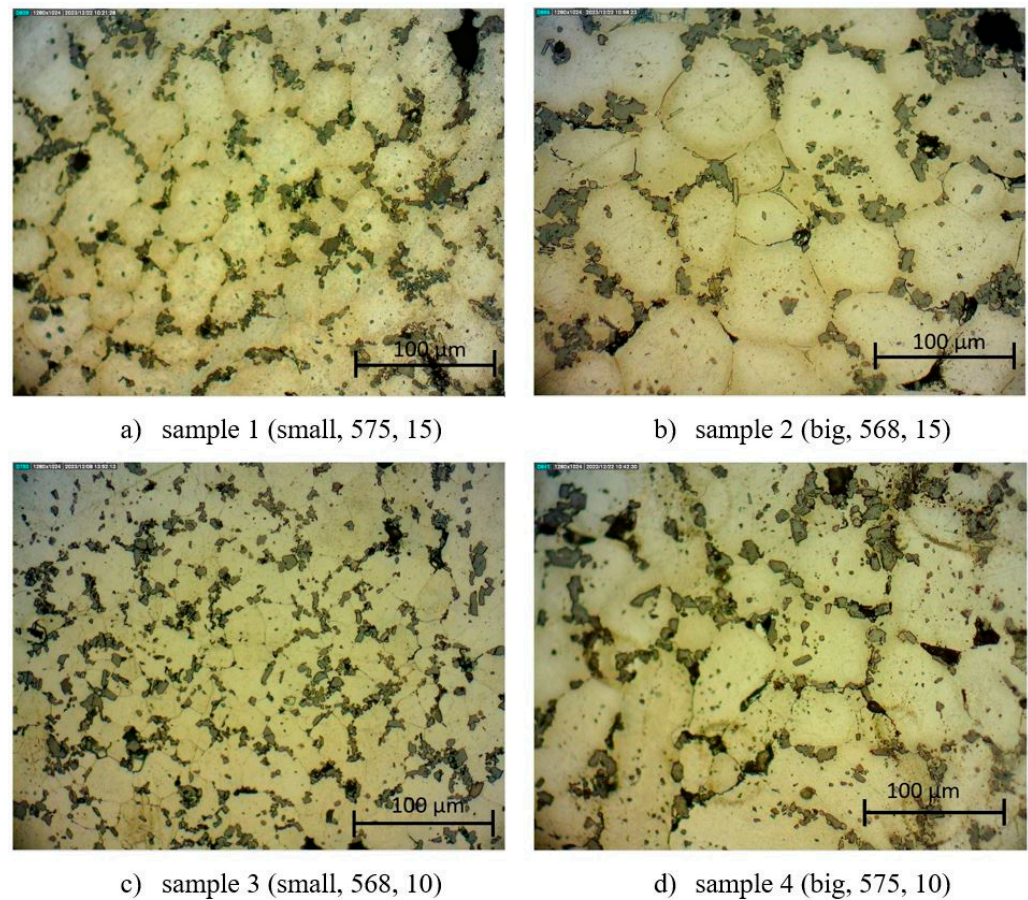


**Figure 8.** Metallography analysis of the specimens prepared according to the Taguchi L4 ( $2^3$ ) experimental plan.

### 3.5. Grey Relation Analysis

In this research, the grey relational analysis was utilized to optimize the multiple characteristics of the thixoformed samples. This was achieved by determining and optimizing a grey relational grade, GRG. In the initial stage, the output parameters were normalized within the range of zero to one to transform the original sequence into a comparable form, i.e., so that the different experimental data could be compared. The normalized values for the globule size followed a lower-a-better criterion, while the circularity, tensile strength, electrical conductivity, and hardness followed a higher-a-better criterion. Both criteria can be respectively expressed as:

$$a_{ij} = \frac{\max b_{ij} - b_{ij}}{\max b_{ij} - \min b_{ij}} \quad (4)$$

$$a_{ij} = \frac{b_{ij} - \min b_{ij}}{\max b_{ij} - \min b_{ij}} \quad (5)$$

where  $a_{ij}$  is the value after the grey relation generation and  $b_{ij}$  is the value of the original data. The subscript  $j$  represents the response and the  $i$  experiment. The smallest value of the original data for the  $j$ th response of experiment  $i$  is denoted by  $\min b_{ij}$ . On the other hand, the largest value of  $b_{ij}$  is denoted by  $\max b_{ij}$ .

The subsequent step involves determining the reference sequence. The reference sequence  $a_{0j}$  is selected when  $a_{ij}$  is equal to 1. Therefore, all other sequences are used for

comparison. Furthermore, the grey relation coefficient,  $x_{ij}$ , is used for determining the closeness to the reference sequence and any other sequence and can be expressed as:

$$x_{ij} = \frac{y_{min} + Zy_{max}}{y_{ij} + Zy_{max}} \quad (6)$$

$$y_{ij} = |a_{0j} - a_{ij}| \quad (7)$$

where  $y_{min} = 0$ ,  $y_{max} = 1$ , and  $Z$  is the distinguishing coefficient and has a value between zero and one. In this study, the value of the distinguishing coefficient was assumed as 0.5. A higher grey relation coefficient indicates a greater similarity between  $a_{0j}$  and  $a_{ij}$ . The absolute difference between the reference sequence and the comparison sequence is denoted by  $y_{ij}$ . The next step was to determine the mean value of  $x_{ij}$ , i.e., to calculate the grey relational grade. The average values of the grey relation coefficient were calculated:

$$y_i = \frac{1}{n} \sum_{j=1}^n x_{ij} \quad (8)$$

where  $y_i$  is grey relation grade (GRG) for the  $i$ th experiment and  $n$  is the number of process responses. GRG quantifies the correlation between  $a_{0j}$  and  $a_{ij}$ . A higher GRG indicates that the corresponding combination of the controllable parameters is closer to the optimum. The experiment with the highest GRG is the most favorable choice (indicated as the first order), Table 6. The grey relation coefficients,  $x_{ij}$ , for each experiment are also presented in Table 6.

**Table 6.** The calculated grey relational coefficients and GRG.

Run	Tensile Strength MPa	Electrical Conductivity %IACS	Hardness HV	GS μm	SF	Grade $y_i$	Grey Order
1	1	0.57	0.33	0.93	0.36	0.64	3
2	0.33	0.33	1	0.33	1	0.60	4
3	0.73	1	0.61	1	0.33	0.73	1
4	0.68	1	0.80	0.45	0.44	0.67	2

According to the results and set selection criteria described above, specimen 3 is the optimum choice in comparison with the other specimens from the Taguchi L4 ( $2^3$ ) experimental plan. Therefore, the suitable temperature to achieve the desirable mechanical and physical properties of the semisolid recycled specimen should be 568 °C and a 10 min heating time for the smaller aluminum waste chips. According to the preliminary results and the literature review, any smaller temperature and holding time will not lead to globule formation; however, in that case, the specimens could exhibit even higher mechanical and physical properties because of a small fraction of the liquid phase during the thixoforming, i.e., the process is similar to forging. Semisolid forging with a small fraction of the liquid phase could be a whole new topic for the semisolid recycling of the small aluminum chips waste for the bought wrought and cast alloys, but it is out of scope for this particular research. Furthermore, a higher thixoforming temperature and, especially, a prolonged holding time led to the mechanical and physical properties decrement. The electrical conductivity decrement in specimen 2 indicated possible excessive porosity development and somewhat reduced the microstructure homogeneity (Table 5 and Figure 8).

To quantify and mathematically express the influence of the input parameters, the mean grey relation grades corresponding to the two levels of the controllable parameters are presented in Table 7. The average grey relational grades for each level of the input parameters are calculated in order to determine the optimum parameters. For instance, the mean grey relation grades for level 1 of the chip size are determined by summing the grades of the 1st and 3rd experiments and dividing the calculated sum by two. The GRG values for

each level of the input parameters were determined using an identical method. A greater GRG value corresponds to a better performance. Therefore, the optimal levels of the process parameters, identified as those yielding the highest grey relation grades, include a small chip size, a lower semisolid temperature (568 °C), and a shorter holding time (10 min). In other words, level 1 is the optimal level for all the process parameters. These optimal levels are highlighted in Table 7. The optimum combination of the controllable parameters is the same as in experiment 3. Implementing these optimal process parameters can enhance the stability of the process and improve the mechanical properties of the thixoformed samples.

**Table 7.** Average grey relational grade by factor level and the optimal levels of the process parameters.

	Chip Size	Temperature	Time
Level 1	<b>0.68779</b>	<b>0.66734</b>	<b>0.70463</b>
Level 2	0.63728	0.65773	0.62045
max-min	0.05051	0.00961	0.08417
rank	2	3	1

The differences between the maximum and the minimum values of the average grey relational grades by the factor level are listed in Table 7. The most influential factor on the performance characteristics was determined by comparing these values. The highest value, 0.08417, indicated that the holding time on the thixoforming temperature had the strongest impact on the multi-performance characteristics compared with the other parameters. Additionally, according to the analysis, the second most influential factor was the aluminum waste chips size and finally the temperature. While the temperature did not impact the experiment concerning multiple performance characteristics, it could potentially affect certain performance characteristics individually. These results are in accordance with the obtained mechanical and physical properties of the specimen summarized in Table 5 and the calculated grey relation grade in Table 6. That is why specimen 4, produced at 575 °C and bigger aluminum waste chips, is ranked second according to Table 6. These results align with the set criteria. If the other criteria were to be set, such as focusing on the mechanical and physical properties without analyzing the grain size and shape, different outcomes would be obtained, which is common for multi-objective optimization.

#### 4. Conclusions

In this research, semisolid recycling of the aluminum machining chips waste is presented. It was proven that the machining chips of the alloy EN AC AlSi9Cu3(Fe) were successfully recycled into thixoformed material using an innovative direct recycling process without a remelting step; therefore, the presented process has the potential for further development. The most important conclusions of the conducted research are as follows:

- Optical and scanning electron microscopy accompanied with energy dispersive spectroscopy showed that a significantly deformed microstructure with extremely refined intermetallic compounds (compared with casted specimens) homogeneously dispersed into the aluminum matrix is obtained utilizing the direct hot extrusion process of the aluminum waste chips.
- Extruded chip-based waste specimens served as thixo (semisolid) feedstock material. During heating in the semisolid temperature range, the feedstock material was able to form a globular microstructure with homogeneously dispersed intermetallic compounds, which preserved the polyhedral and refined appearance after the thixoforming process.
- The mechanical and physical properties of the obtained semisolid recycled specimens are comparable with the as-casted ingot specimen.
- The Taguchi method and multi-objective optimization enabled optimal parameters selection among different thixoforming temperatures, holding times in semisolid

temperature range, and aluminum waste chips size. Finally, a 568 °C thixoforming temperature, a 10 min holding time, and smaller-sized aluminum chips resulted in a semisolid recycled specimen that had a tensile strength, electrical conductivity, and hardness of 250 MPa, 29.42%IACS, and 88.68 HV, respectively. The same specimen had a 35.52 µm average globule size and a 0.74 circularity shape factor, which falls into the desirable range.

**Author Contributions:** Conceptualization, J.K. and B.L.; methodology, J.K. and I.D.L.; software, J.K. and I.D.L.; validation, J.K. and I.D.L.; formal analysis, J.K., M.B. and I.D.L.; investigation, J.K.; resources, B.L.; data curation, J.K., I.D.L. and M.B.; writing—original draft preparation, J.K. and I.D.L.; writing—review and editing, J.K. and I.D.L.; visualization, J.K. and M.B.; supervision, B.L.; project administration, J.K. and B.L.; funding acquisition, B.L. All authors have read and agreed to the published version of the manuscript.

**Funding:** This work was financially supported by the Croatian Science Foundation through the project recycling of aluminum alloys in the solid and semisolid states (IP-2020-02-8284).

**Data Availability Statement:** The raw data supporting the conclusions of this article will be made available by the authors on request.

**Conflicts of Interest:** Author Martin Bilušić was employed by the company AluTech. The remaining authors declare that the research was conducted in the absence of any commercial or financial relationships that could be construed as a potential conflict of interest.

## References

1. Deepak Kumar, S.; Ghose, J.; Mandal, A. Thixoforming of Light-Weight Alloys and Composites: An Approach toward Sustainable Manufacturing. In *Sustainable Engineering Products and Manufacturing Technologies*; Kumar, K., Zindani, D., Davim, P., Eds.; Academic Press: Cambridge, MA, USA, 2019; pp. 25–43, ISBN 9780128165645.
2. Li, G.; Qu, W.Y.; Luo, M.; Cheng, L.; Guo, C.; Li, X.; Xu, Z.; Hu, X.; Li, D.; Lu, H.; et al. Semi-Solid Processing of Aluminum and Magnesium Alloys: Status, Opportunity, and Challenge in China. *Trans. Nonferrous Met. Soc. China* **2021**, *31*, 3255–3280. [\[CrossRef\]](#)
3. Hu, Y.; Liu, Y. Constitutive Behavior of Semi-Solid Al80Mg5Li5Zn5Cu5 Light-Weight High Entropy Alloy. *J. Mater. Res. Technol.* **2024**, *29*, 5713–5720. [\[CrossRef\]](#)
4. Fabrizi, A.; Capuzzi, S.; De Mori, A.; Timelli, G. Effect of T6 Heat Treatment on the Microstructure and Hardness of Secondary AlSi9Cu3(Fe) Alloys Produced by Semi-Solid SEED Process. *Metals* **2018**, *8*, 750–768. [\[CrossRef\]](#)
5. Rogal, Ł. Critical Assessment: Opportunities in Developing Semi-Solid Processing: Aluminium, Magnesium, and High-Temperature Alloys. *Mater. Sci. Technol.* **2017**, *33*, 759–764. [\[CrossRef\]](#)
6. Zhang, Z.; Huang, X.; Yang, F.; Zhang, S.; Fu, J. Effect of La Addition on Semi-Solid Microstructure Evolution of Mg-7Zn Magnesium Alloy. *China Foundry* **2022**, *19*, 403–410. [\[CrossRef\]](#)
7. Wang, J.; Phillion, A.B.; Lu, G. Development of a Visco-Plastic Constitutive Modeling for Thixoforming of AA6061 in Semi-Solid State. *J. Alloys Compd.* **2014**, *609*, 290–295. [\[CrossRef\]](#)
8. Salleh, M.S.; Omar, M.Z.; Syarif, J.; Mohammed, M.N. An Overview of Semisolid Processing of Aluminium Alloys. *ISRN Mater. Sci.* **2013**, *2013*, 679820. [\[CrossRef\]](#)
9. Ragab, K.A.; Bouazara, M.; Bouaicha, A.; Allaoui, O. Microstructural and Mechanical Features of Aluminium Semi-Solid Alloys Made by Rheocasting Technique. *Mater. Sci. Technol.* **2017**, *33*, 646–655. [\[CrossRef\]](#)
10. Kirkwood, D.; Kapranos, P.; Suéry, M.; Atkinson, H.V.; Young, K.P. *Semi-Solid Processing of Alloys*; Springer: Berlin, Germany, 2010; ISBN 9783642007057.
11. Proni, C.T.W.; Torres, L.V.; Haghayeghi, R.; Zoqui, E.J. ECAP: An Alternative Route for Producing AlSiCu for Use in SSM Processing. *Mater. Charact.* **2016**, *118*, 252–262. [\[CrossRef\]](#)
12. Das, P.; Kumar, M.; Samanta, S.K.; Dutta, P.; Ghosh, D. Semisolid Processing of A380 Al Alloy Using Cooling Slope. *Mater. Manuf. Process.* **2014**, *29*, 422–428. [\[CrossRef\]](#)
13. Gecu, R.; Acar, S.; Guler, K.A. Microstructural Evaluation of T6-Treated A380 Alloy Manufactured by Semi-Solid Metal Casting. In Proceedings of the International Conference on Engineering Technology and Innovation, Sarajevo, Bosnia and Herzegovina, 22–26 March 2017.
14. Parshizfard, E.; Shabestari, S.G. An Investigation on the Microstructural Evolution and Mechanical Properties of A380 Aluminum Alloy during SIMA Process. *J. Alloys Compd.* **2011**, *509*, 9654–9658. [\[CrossRef\]](#)
15. Gencalp, S.; Saklakoglu, N. Semisolid Microstructure Evolution during Cooling Slope Casting under Vibration of A380 Aluminum Alloy. *Mater. Manuf. Process.* **2010**, *25*, 943–947. [\[CrossRef\]](#)



16. Guo, H.; Yang, X.; Hu, B.; Zhu, G. Rheo-Diecasting Process for Semi-Solid Aluminum Alloys. *J. Wuhan Univ. Technol. Mater. Sci. Ed.* **2007**, *22*, 590–595. [\[CrossRef\]](#)
17. Chen, Y.; Cao, M.; Li, H.; Wang, Y.; Zhang, Q. Multi-Physics Coupling Simulation Investigation of Semi-Solid A380 Aluminum Alloy during Intermediate Frequency Electromagnetic Stirring Process. *Int. J. Adv. Manuf. Technol.* **2023**, *125*, 4329–4339. [\[CrossRef\]](#)
18. Jahare, M.H.; Idris, M.H.; Wan Ali, W.F.F. Solid Fraction Effect on Solidification of Semisolid Forging A380 Alloy. *Mater. Manuf. Process.* **2022**, *37*, 230–239. [\[CrossRef\]](#)
19. Gudić, S.; Vrsalović, L.; Krolo, J.; Nagode, A.; Dumanić Labetić, I.; Lela, B. Corrosion Behaviour of Recycled Aluminium AlSi9Cu3(Fe) Machining Chips by Hot Extrusion and Thixoforming. *Sustainability* **2024**, *16*, 1358–1377. [\[CrossRef\]](#)
20. Xu, R.; Wang, W.; Zheng, H.; Liu, Z.; Cui, X.; Han, Y.; Ma, Y.; Feng, S.Y. Study on Preparation Process and Performance Properties of High-Solid-Fraction Semi-Solid A380 Alloy. *Int. J. Met.* **2023**, 1–11. [\[CrossRef\]](#)
21. Fu, J.L.; Jiang, H.J.; Wang, K.K. Influence of Processing Parameters on Microstructural Evolution and Tensile Properties for 7075 Al Alloy Prepared by an ECAP-Based SIMA Process. *Acta Metall. Sin.* **2018**, *31*, 337–350. [\[CrossRef\]](#)
22. Meshkabadi, R.; Faraji, G.; Javdani, A.; Pouyafar, V. Combined Effects of ECAP and Subsequent Heating Parameters on Semi-Solid Microstructure of 7075 Aluminum Alloy. *Trans. Nonferrous Met. Soc. China* **2016**, *26*, 3091–3101. [\[CrossRef\]](#)
23. Yang, Z.; Wang, K.; Yang, Y. Optimization of ECAP—RAP Process for Preparing Semisolid Billet of 6061 Aluminum Alloy. *Int. J. Miner. Metall. Mater.* **2020**, *27*, 792–800. [\[CrossRef\]](#)
24. Ch, S.; Venkateswarlu, G.; Davidson, M.J. Optimization of Process Parameters on the Mechanical Properties of Semi-Solid Extruded AA2017 Alloy Rods. *Int. J. Mater. Form. Mach. Process.* **2019**, *6*, 1–14. [\[CrossRef\]](#)
25. Rodrigues Dantas, A.V.; Brollo, G.L.; Tamayo, D.V.; Zoqui, E.J. Thixoforming of an Al-Si-Zn-Mg Alloy—Thermodynamic Characterization, Microstructural Evolution and Rheological Behavior. *Mater. Res.* **2021**, *24*, e20200313. [\[CrossRef\]](#)
26. Wang, K.; Hu, S.; Wang, T.; Xie, W.; Guo, T.; Li, F.; Luo, R. Microstructural Evolution and Mechanical Properties of 7075 Aluminium Alloy during Semi-Solid Compression Deformation. *Crystals* **2022**, *12*, 1119–1133. [\[CrossRef\]](#)
27. Paraskevas, D.; Vanmeensel, K.; Vleugels, J.; Dewulf, W.; Deng, Y.; Duflou, J.R. Spark Plasma Sintering as a Solid-State Recycling Technique: The Case of Aluminum Alloy Scrap Consolidation. *Materials* **2014**, *7*, 5664–5687. [\[CrossRef\]](#) [\[PubMed\]](#)
28. Krolo, J.; Lela, B.; Grgić, K.; Jozić, S. Production of Closed-Cell Foams out of Aluminum Chip Waste: Mathematical Modeling and Optimization. *Metals* **2022**, *12*, 933–950. [\[CrossRef\]](#)
29. Jozić, S.; Lela, B.; Krolo, J.; Jakovljević, S. Production of Open-Cell Metal Foams by Recycling of Aluminum Alloy Chips. *Materials* **2023**, *16*, 3930–3947. [\[CrossRef\]](#)
30. El Mehtedi, M.; Buonadonna, P.; Carta, M.; El Mohtadi, R.; Mele, A.; Morea, D. Sustainability Study of a New Solid-State Aluminum Chips Recycling Process: A Life Cycle Assessment Approach. *Sustainability* **2023**, *15*, 11434–11448. [\[CrossRef\]](#)
31. Zhang, Z.; Liang, J.; Xia, T.; Xie, Y.; Chan, S.L.I.; Wang, J.; Zhang, D. Effects of Oxide Fragments on Microstructure and Mechanical Properties of AA6061 Aluminum Alloy Tube Fabricated by Thermomechanical Consolidation of Machining Chips. *Materials* **2023**, *16*, 1384–1397. [\[CrossRef\]](#)
32. Feng, Z.; David, S.A.; Manchiraju, V.K.; Frederick, D.A.; Thomas, W. Friction Extrusion: Solid-State Metal Synthesis and Recycling in Sustainable Manufacturing. *JOM* **2023**, *75*, 2962–2973. [\[CrossRef\]](#)
33. Stacey, M. *Aluminium Recyclability and Recycling: Towards Sustainable Cities*, 1st ed.; Cwningen Press: London, UK, 2015; ISBN 9780993016219.
34. Paraskevas, D.; Kellens, K.; Dewulf, W.; Duflou, J.R. Environmental Modelling of Aluminium Recycling: A Life Cycle Assessment Tool for Sustainable Metal Management. *J. Clean. Prod.* **2015**, *105*, 357–370. [\[CrossRef\]](#)
35. Czerwinski, F. *Magnesium Injection Molding*; Springer: New York, NY, USA, 2008; ISBN 978-0-387-72528-4.
36. Czerwinski, F. The Oxidation Behaviour of an AZ91D Magnesium Alloy at High Temperatures. *Acta Mater.* **2002**, *50*, 2639–2654. [\[CrossRef\]](#)
37. Wang, Z.Y.; Ji, Z.S.; Sun, L.X.; Xu, H.Y. Microstructure of Semi-Solid ADC12 Aluminum Alloy Adopting New SIMA Method. *Trans. Nonferrous Met. Soc. China* **2010**, *20*, 744–748. [\[CrossRef\]](#)
38. Wang, Z.; Ji, Z.; Hu, M.; Xu, H. Evolution of the Semi-Solid Microstructure of ADC12 Alloy in a Modified SIMA Process. *Mater. Charact.* **2011**, *62*, 925–930. [\[CrossRef\]](#)
39. Wang, F.; Zhang, W.Q.; Xiao, W.L.; Yamagata, H.; Ma, C.L. Microstructural Evolution during Reheating of A356 Machining Chips at Semisolid State. *Int. J. Miner. Metall. Mater.* **2017**, *24*, 891–900. [\[CrossRef\]](#)
40. Wang, Y.; Hu, M.; Xu, H.; Ji, Z.; Wen, X.; Liu, X. Effect of Isothermal Process Parameters on Semi-Solid Microstructure of Chip-Based Al-Cu-Mn-Ti Alloy Prepared by SIMA Method. *Mod. Phys. Lett. B* **2020**, *34*, 20503856. [\[CrossRef\]](#)
41. Son, Y.G.; Jung, S.S.; Park, Y.H.; Lee, Y.C. Effect of Semi-Solid Processing on the Microstructure and Mechanical Properties of Aluminum Alloy Chips with Eutectic Mg<sub>2</sub>Si Intermetallics. *Metals* **2021**, *11*, 1414–1424. [\[CrossRef\]](#)
42. Dumanić, I.; Jozić, S.; Bajić, D.; Krolo, J. Optimization of Semi-Solid High-Pressure Die Casting Process by Computer Simulation, Taguchi Method and Grey Relational Analysis. *Int. J. Met.* **2021**, *15*, 108–118. [\[CrossRef\]](#)
43. Eftekhari, A.H.; Sadrossadat, S.M.; Reihanian, M. Statistical Optimization of Electromagnetic Stirring Parameters for Semisolid AM60 Slurry Using Taguchi-Based Grey Relational Analysis. *Int. J. Met.* **2022**, *16*, 212–222. [\[CrossRef\]](#)
44. Nakowong, K.; Sillapasa, K. Optimized Parameter for Butt Joint in Friction Stir Welding of Semi-Solid Aluminum Alloy 5083 Using Taguchi Technique. *J. Manuf. Mater. Process.* **2021**, *5*, 88–109. [\[CrossRef\]](#)

45. Hirt, G.; Kopp, R. *Thixoforming: Semi-Solid Metal Processing*; John Wiley & Sons: Weinheim, Germany, 2009; ISBN 9783527322046.
46. Nafisi, S.; Ghomashchi, R. *Semi-Solid Processing of Aluminum Alloys*; Springer International Publishing: Cham, Switzerland, 2016; ISBN 9783319403359.
47. Saha, P.K. *Aluminum Extrusion Technology*; ASM International: Materials Park, OH, USA, 2000; ISBN 978-1-62708-336-2.
48. Cooper, D.R.; Allwood, J.M. The Influence of Deformation Conditions in Solid-State Aluminium Welding Processes on the Resulting Weld Strength. *J. Mater. Process. Technol.* **2014**, *214*, 2576–2592. [[CrossRef](#)]
49. Yuan, Z.; Guo, Z.; Xiong, S.M. Effect of As-Cast Microstructure Heterogeneity on Aging Behavior of a High-Pressure Die-Cast A380 Alloy. *Mater. Charact.* **2018**, *135*, 278–286. [[CrossRef](#)]
50. Gencalp Irizalp, S.; Saklakoglu, N. Effect of Fe-Rich Intermetallics on the Microstructure and Mechanical Properties of Thixoformed A380 Aluminum Alloy. *Eng. Sci. Technol. Int. J.* **2014**, *17*, 58–62. [[CrossRef](#)]
51. Birol, Y. Forming of AlSi8Cu3Fe Alloy in the Semi-Solid State. *J. Alloys Compd.* **2009**, *470*, 183–187. [[CrossRef](#)]
52. Liu, Y.; Jiang, J.; Xiao, G.; Zhang, Y.; Huang, M.; Wang, Y. Effects of Temperature and Time on Three-Dimensional Microstructural Evolution of Semi-Solid 2A14 Aluminum Alloy during Short Process Preparation of Semi-Solid Billets. *Trans. Nonferrous Met. Soc. China* **2022**, *32*, 2091–2109. [[CrossRef](#)]
53. HRN EN ISO 6507-1:2018; Metallic Materials—Vickers Hardness Test—Part 1: Test Method (ISO 6507-1:2018; EN ISO 6507-1:2018). Croatia Standards Institute: Zagreb, Croatia, 2018. Available online: <https://repozitorij.hzn.hr/norm/HRN+EN+ISO+6507-1%3A2018> (accessed on 20 January 2023).
54. EN ISO10002-1; Metallic Materials—Tensile Testing—Part 1: Method of Test at Room Temperature. Croatia Standards Institute: Zagreb, Croatia, 2001. Available online: <https://repozitorij.hzn.hr/norm/HRN+EN+10002-1%3A2008> (accessed on 15 March 2023).
55. Farina, M.E.; Bell, P.; Ferreira, C.R.F.; Dedavid, B.A. Effects of Solidification Rate in the Microstructure of Al-Si5Cu3 Aluminum Cast Alloy. *Mat. Res.* **2017**, *20*, 273–278. [[CrossRef](#)]
56. Yang, W.C.; Gao, F.; Ji, S.X. Formation and Sedimentation of Fe-Rich Intermetallics in Al-Si-Cu-Fe Alloy. *Trans. Nonferrous Met. Soc. China* **2015**, *25*, 1704–1714. [[CrossRef](#)]
57. Krolo, J.; Gudić, S.; Vrsalović, L.; Lela, B.; Dadić, Z. Fatigue and Corrosion Behavior of Solid-State Recycled Aluminum Alloy EN AW 6082. *J. Mater. Eng. Perform.* **2020**, *29*, 4310–4321. [[CrossRef](#)]
58. Lipińska, M.; Bazarnik, P.; Lewandowska, M. The Influence of Severe Plastic Deformation Processes on Electrical Conductivity of Commercially Pure Aluminium and 5483 Aluminium Alloy. *Arch. Civ. Mech. Eng.* **2016**, *16*, 717–723. [[CrossRef](#)]

**Disclaimer/Publisher's Note:** The statements, opinions and data contained in all publications are solely those of the individual author(s) and contributor(s) and not of MDPI and/or the editor(s). MDPI and/or the editor(s) disclaim responsibility for any injury to people or property resulting from any ideas, methods, instructions or products referred to in the content.